J. Fluid Mech. (2001), *vol.* 437, *pp.* 283–299. Printed in the United Kingdom

Numerical study of the motions within a slowly precessing sphere at low Ekman number

By JÉRÔME NOIR, D. JAULT AND P. CARDIN

LGIT, CNRS, Université Joseph Fourier, BP 53, 38041 Grenoble, France

(Received 9 September 2000 and in revised form 27 December 2000)

A geostrophic circulation and a pair of oblique oscillating shear layers arise in a spherical fluid cavity contained in a slowly precessing rigid body. Both are caused by the breakdown of the Ekman boundary layer at two critical circles. We rely on numerical modelling to characterize these motions for very small Ekman numbers. Both the $O(E^{1/5})$ amplitude of the velocity in the oscillating shear layer and the width (also $O(E^{1/5})$) of these oblique layers are the result of influx into the interior from the regions where the Ekman layer breaks down. The oscillating motions are confined to narrow shear layers and their amplitude decays exponentially away from the characteristic surfaces. Nonlinear interactions inside the boundary layer drive the geostrophic shear layer attached to the critical circles. This steady layer, again of $O(E^{1/5})$ thickness, contains $O(E^{-3/10})$ velocities. Our results are in good agreement with the experimental measurement by Malkus of the geostrophic velocity arising in a slowly precessing spheroid.

1. Introduction

Motions, with diurnal period, are produced, inside the Earth's fluid core, by the slow precession of the Earth's rotation axis. The amplitude of these motions is unknown as they do not cause changes in the magnetic field measured at the Earth's surface. They have been neglected in numerical studies of the geodynamo because the magnetic diffusion time of the Earth's core is large compared to diurnal periods. However, nonlinear interaction between these motions may yield slowly varying flows that can play a role in the generation of the magnetic field (Malkus 1968).

In the absence of either direct or indirect observations, laboratory experiments, theoretical investigations and numerical calculations have been particularly important for our understanding of fluid motions inside the Earth's core due to the precession of the mantle. Neglecting viscous friction at the core–mantle boundary, Poincaré (1910) calculated the response of the fluid to the precession of its spheroidal boundary. It is little different from a rotation about an equatorial axis, the $(2, 1, 1)$ mode, as denoted in the classification of Greenspan (1968) for spherical inertial modes, and it has to be considered in studies of nutation of the Earth's axis of rotation. The correction to this mode due to viscous friction at the boundary is not easily calculated because the Ekman layer of width $E^{1/2}$ (where E is the Ekman number) is singular at the critical circles. There, the viscous term does not enter the balance of forces at the main order. As a consequence, the radial lengthscale is large compared to $E^{1/2}$. Roberts & Stewartson (1963) found indeed that the depth of the boundary layer scales as $E^{2/5}$

in a region of $O(E^{1/5})$ dimension around the critical latitude (at 30° latitude in the sphere). Then, Busse (1968) calculated the viscous correction to the Poincaré motion in a precessing spheroid. He obtained his solution by assuming a double expansion involving two small parameters $E^{1/2}$ and ε, the amplitude of the boundary-layer flow. Busse found that at the order $E^{1/2}\ \varepsilon$ the interior flow can be expressed as $\boldsymbol{\omega} \times \boldsymbol{r}$, where $\boldsymbol{r}$ is the position vector and $\boldsymbol{\omega}$ is a rotation vector, which is constant in the frame of reference which rotates with the precession rate. He showed that the critical circles at which the Ekman layer breaks down occur with respect to $\boldsymbol{\omega}$.

The interior sees the breakdown of the $E^{1/2}$-layer as a singularity since there the flow emitted by the boundary layer does not scale as $E^{1/2}$. Kerswell (1995) realized that the Ekman layer breakdown spawns an inertial wave into the interior and he conjectured that the scaling of its wavelength stems directly from the $O(E^{1/5})$ size of the source. The scaling of the influx into the interior from the critical zones of the boundary layer was given by Stewartson & Roberts (1963), in their study of the motion in a precessing spheroid. It is $O(E^{1/5})$ instead of $O(E^{1/2})$ away from the singularities. We may then anticipate that the velocity in the oscillating shear layers scale also as $E^{1/5}$ (rather than $E^{3/10}$ as suggested by Kerswell). The singularity is propagated along the characteristic surfaces of the equation governing inertial waves with diurnal period. The characteristic surfaces are cones symmetric about the fluid's rotation axis which have semi-angle 30°. In a sphere, there are two characteristic surfaces each associated with one of the two critical circles (Hollerbach & Kerswell 1995). Both cones meet the rotation axis at a pole on the boundary and this makes the spherical problem special. Numerical modelling can validate the conjectures listed above about the behaviour of the solution as $E \to 0$. We give also particular attention to the decay of the shear away from the characteristics attached to the Ekman layer breakdown. We rely, for this study, on the spin-over problem, which may be described as a linearization of the precession problem.

However, explaining the geostrophic circulation exhibited by Malkus (1968) necessitates nonlinear studies. Malkus was particularly interested by the turbulence that he witnessed at large precession rate of an oblate spheroid but he also visualized, at smaller precession rate, a geostrophic circulation. To date, the Malkus' observations give the only quantitative measure of the geostrophic circulation arising in a precessing spheroid (see our figure 8). Greenspan (1969) proved that the nonlinear interaction of inviscid inertial modes cannot produce a geostrophic flow. This highlighted the importance of the study by Busse (1968). This author showed that nonlinear interactions between different parts of the boundary-layer flow, of amplitude ε, yield, at the order ε^2, a geostrophic shear extending into the interior. The findings of Busse explained well the experimental results of Malkus (1968), notwithstanding the divergence of the solution at the critical circles where the $O(E^{1/2})$ scaling for the width of the Ekman layer fails. In order to remedy the divergence of the solution found by Busse, a study of the nonlinearities in the boundary layer at the two critical circles is required. The complete asymptotic theory appears difficult to obtain. Our numerical investigation of the full precession problem allows us nevertheless to outline such a study. We propose asymptotic laws for the thickness of the axial shear layer and for the velocities that it contains. As showed by Busse, we do not lose generality here by studying only the spherical case. It enables us also to describe finite viscosity effects, such as possible nonlinear interaction of the motions inside the oblique shear layers.

The inertial waves, that make the shear layers, are not much affected by viscous forces because their lengthscale is large compared to the $E^{1/3}$ natural scale. Away from the critical circles, they obey the no-penetration condition (at the order $E^{1/2}$),

crucial to Greenspan's proof. As a result, their nonlinear interaction does not yield, in the limit of vanishing viscosity, a steady geostrophic circulation, notwithstanding the geostrophic shear attached to the critical circles and pointed out by Busse (1968). On the other hand, Vanyo *et al.* (1995) have observed several axial shear structures in an oblate precessing spheroid filled with water (their figure 2). Because of light refraction at the interface between Plexiglas and air, the photographs of Vanyo *et al.* (1995) do not show the shear predicted by Busse and observed by Malkus but instead axial shear layers occurring at smaller distances to the rotation axis. Hence, Hollerbach & Kerswell (1995), in the course of their investigation of the unforced spin-over mode in a sphere, suggested that, in addition to the geostrophic shear found by Busse, which can be explained by the breakdown of the Ekman layer only, other shear zones arise as the result of nonlinear interaction between the inertial waves in the interior. If true, it is a finite viscosity effect. Investigating the precessionally forced mode in the sphere allows us to question the suggestion put forward by Hollerbach & Kerswell to explain these structures. The ellipticity of the oblate spheroid that has been used in the experiment of Vanyo *et al.* (1995) is indeed small compared to $E^{1/5}$. We may thus consider it spherical. Finally, a recent study by Tilgner (1999*b*) of the flow in a precessing spherical shell is best discussed, in the light of our results, at the end of the article.

Section 2 describes the equations that are solved and the numerical method. Section 3 treats the linear problem. It is focused on the scaling of the inertial waves emitted by the singularity in the Ekman layer. Results about the full precession problem are given in § 4. We treat it as an initial-value problem. We conclude with a discussion that includes a comparison between the quantitative measurements of Malkus (1968) and our numerical solution. Possible implications for Earth's core dynamics are considered also.

2. Equations of the problem

An incompressible fluid of kinematic viscosity ν is enclosed in a spherical container of radius R. The sphere is spinning with a frequency ω_c along $\hat{\boldsymbol{k}}_c$, and precessing at $\omega_c\Omega_p$ along $\hat{\boldsymbol{k}}_p$. Units of length and time are chosen as R and ω_c^{-1}, respectively, $E = \nu/\omega_c R^2$ is the Ekman number. Following Busse (1968), we assume that the main response of the fluid to the precession of the container is a solid-body rotation $\boldsymbol{\omega} \times \boldsymbol{r}$ on which a secondary flow is superimposed and that the rotation vector $\boldsymbol{\omega}$ is also precessing at $\omega_c\Omega_p$. We write the momentum equation in a referential frame attached to the solid-body rotation of the fluid. Including the centrifugal force in the reduced pressure φ, the momentum equation for $\boldsymbol{u}$ reads:

$$\frac{\partial \boldsymbol{u}}{\partial t} + 2(\Omega_p \hat{\boldsymbol{k}}_p(t) + \boldsymbol{\omega}) \times \boldsymbol{u} + (\Omega_p \hat{\boldsymbol{k}}_p(t) \times \boldsymbol{\omega}) \times \boldsymbol{r} + (\boldsymbol{u} \cdot \nabla)\boldsymbol{u} = -\nabla\varphi + E\nabla^2 \boldsymbol{u}. \tag{2.1}$$

Boundary conditions are no-slip and no-penetration at $r = 1$:

$$\boldsymbol{u} = (\hat{\boldsymbol{k}}_c(t) - \boldsymbol{\omega}) \times \boldsymbol{r}. \tag{2.2}$$

The vectors $\hat{\boldsymbol{k}}_p(t)$ and $\hat{\boldsymbol{k}}_c(t)$ are time-dependent.

Equation (2.1) is invariant under parity transformation $P : \boldsymbol{r} \to -\boldsymbol{r}$, $\boldsymbol{u} \to -\boldsymbol{u}$. We can thus divide the solutions of this equation into two sets. The forcing at the boundary is symmetric under parity. Antisymmetric motions may thus arise only as a consequence of a bifurcation. Hence, we leave aside this set of velocity fields in § 3.

We have found that the choice of the rotation vector $\boldsymbol{\omega}$ is crucial to obtain an

accurate solution of the precession problem. To obtain the same level of accuracy, a much larger truncation level M (see (A 2) and (A 3)) would be required if the choice of the rotation vector were not appropriate. We start our time-stepping calculations with the rotation vector analytically determined by Busse (1968). Then, we correct it by the residual solid-body rotation that we have inferred numerically. In addition, this procedure also makes the analysis of the results easier as the location of the different shear layers are determined with respect to $\boldsymbol{\omega}$. The final solution is steady in the frame of reference that rotates with the precession rate. Time integration is of the order of a few spin-up times $E^{-1/2}\omega_c^{-1}$. Other details of the numerical method are left for the Appendix.

3. Viscous correction to the spinover mode

We study first the linear problem. Neglecting the nonlinear terms allows us to calculate the solution for very low values of the Ekman number (down to $E = 10^{-8}$) and to determine the structure of the shear layer spawned by the Ekman layer breakdown at 30° latitude. Let us again consider a fluid rotating with its spherical container at $\boldsymbol{\omega}_c$. We assume that the axis of rotation of the shell is suddenly tilted by an infinitesimal quantity, so that the problem is linear. The momentum equation in the coordinate system rotating with $\boldsymbol{\omega}_c$ is:

$$\frac{\partial \boldsymbol{u}}{\partial t} + 2\hat{\boldsymbol{k}}_c \times \boldsymbol{u} = -\nabla\varphi + E\nabla^2\boldsymbol{u}, \tag{3.1}$$

with the rigid boundary condition:

$$\boldsymbol{u} = 0. \tag{3.2}$$

It amounts to equation (2.1) with $\Omega_p \ll 1$, $\boldsymbol{\omega} = \hat{\boldsymbol{k}}_c$ and the nonlinear terms neglected. We consider as initial condition a differential rotation between the fluid and the solid container around an axis in the equatorial plane. Then, the primary velocity is a rotation about an equatorial axis fixed in the inertial space, referred to as the $(2,1,1)$ mode by Greenspan (1968). The rotation vector is denoted by $\boldsymbol{\omega}_1$. We look on the viscous correction to this inviscid mode. Only ($m = 1$) terms need to be considered (see (A 4) for the definition of m).

3.1. *The* $(2,1,1)$ *mode*

Taking into account the viscous boundary layer, Greenspan gives the exponential decay $-2.62\,E^{1/2}$ of the amplitude of the mode $(2,1,1)$ and the viscous correction $-0.259\,E^{1/2}$ to its eigenfrequency. In the numerical study of Hollerbach & Kerswell (1995) as in ours, the observed decay factor seems to approach asymptotically the coefficient determined analytically. Figure 1 shows the decay factor λ for different Ekman numbers. It transpires that the expansion (Greenspan 1968) in powers of $E^{1/2}$ holds at first order. The oblique shear layers studied below do not have a significant effect on the viscous damping of the spin-over mode. As a result, we may expect that the expression (see equation (4.1)) given by Busse (1968) for the solid-body rotation of a fluid enclosed in a precessing spherical cavity is very accurate also. Indeed, Busse has assumed the same expansion in powers of $E^{1/2}$ to determine the boundary-layer effects.

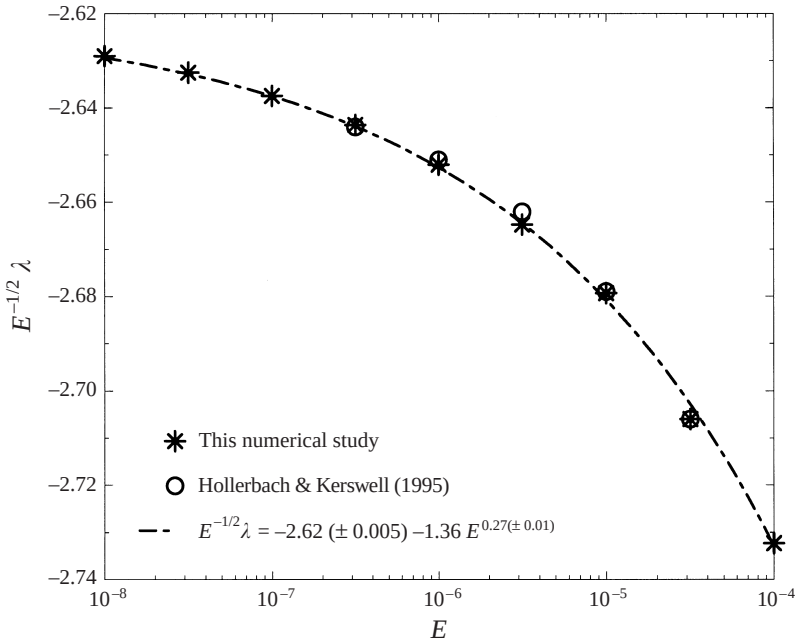

FIGURE 1. Viscous decay of the mode (2, 1, 1). An exponential fit to the calculated decay rate λ is also reported.

3.2. *The internal shear layer*

The numerical calculations of Hollerbach & Kerswell (1995) have shown internal shear zones spawned by singularities in the Ekman boundary layer at the critical latitude of 30°. Kerswell (1995) argued that the $O(E^{1/5})$ width of the region where the Ekman layer breaks down determines the lengthscale of the shear layer because it is larger than the $O(E^{1/3})$ natural lengthscale. In order to study the shear layer, we first remove a solid-body rotation about an equatorial axis (the $(2, 1, 1)$ component of the velocity field). In this subsection, the velocity unit is $\omega_1 R$. Figure 2 shows the three components of the residual velocity for Ekman numbers ranging from 10^{-6} to 10^{-8}. Internal shear layers organized along characteristic surfaces of equation (3.1), which is hyperbolic for diurnal motions, are clearly visible.

Let us consider a cross-section of the internal shear zone. At the constant 30° latitude, the velocity components are given as a function of radius (figure 3). With this choice, both u_θ and u_ϕ are parallel to the characteristic surface ((r, θ, ϕ) are spherical coordinates). The cross-section is directed along the wave vector and the shear layer is centred on $(r = 0.5)$, in the meridional plane defined by $\hat{\boldsymbol{k}}_c$ and $\boldsymbol{\omega}_1$. We consider that the wavelength scales as $E^{1/5}$, as anticipated by Kerswell, with a prefactor of the order of the sphere radius. The velocities tangential to the characteristic cones scale also as $E^{1/5}$ and decay exponentially away from the shear layers. In order to illustrate these effects, we have rescaled both the distance from the shear layer $r^* - 0.5 = E^{-1/5}(r - 0.5)$ and the velocity amplitude $u^* = E^{-1/5}u$ (figure 3). Table 1 shows the extrema of u_ϕ as a function of the distance to the characteristic surface. We find that the decay exponent is $O(E^{-1/5})$, as the wavenumber. In each meridional plane, the velocity is almost invariant along the characteristic lines. It changes as $s^{-1/2}$

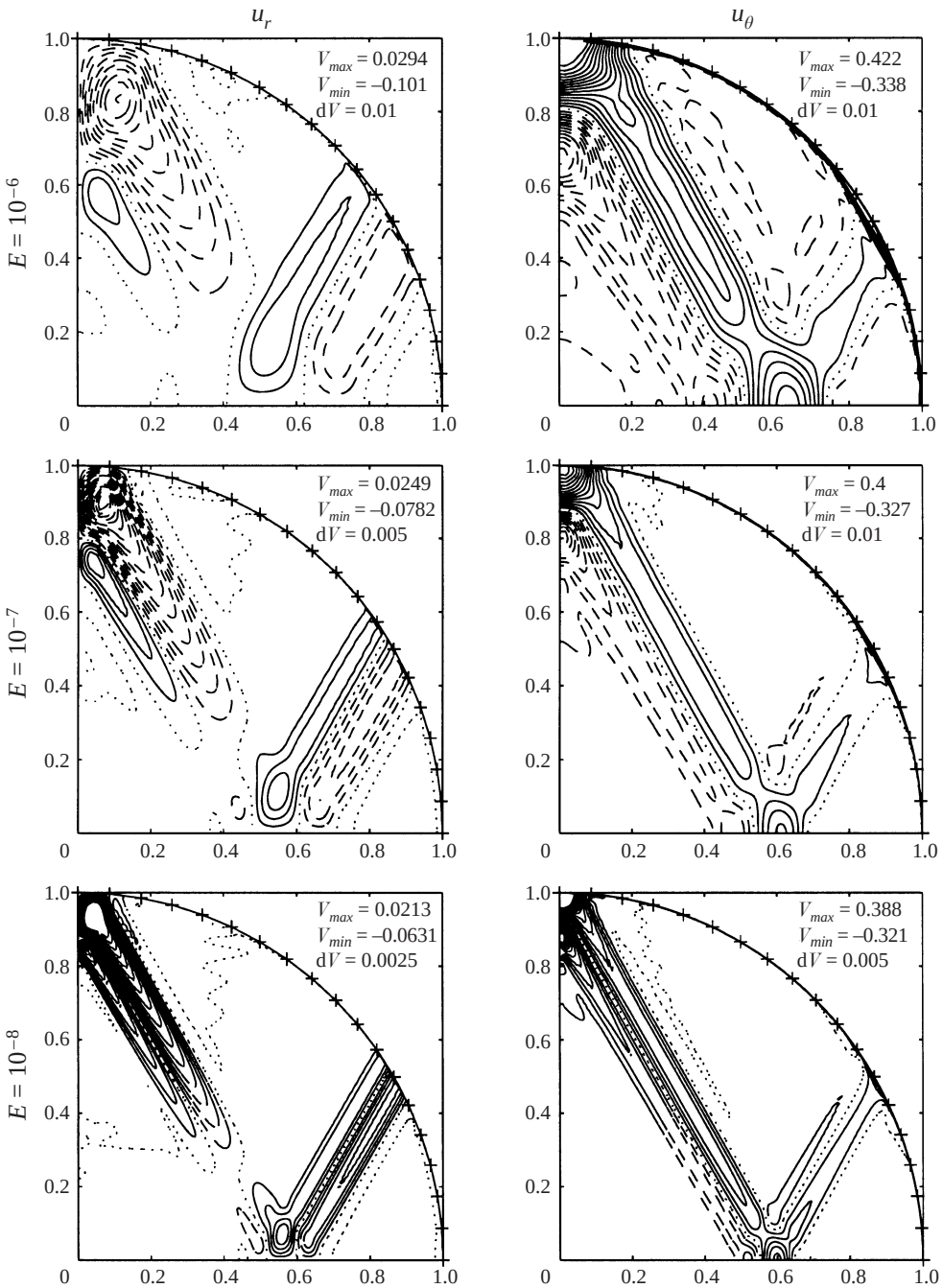

FIGURE 2. For caption see facing page.

(Rieutord & Valdetarro 1997), where s is the cylindrical radius. It is dictated by the radial velocity either entering or leaving the boundary layer at the critical circles. Let us recall, for future reference, the elucidation of this boundary layer by Roberts & Stewartson (1963).

These authors write the momentum equation in the boundary layer near a critical

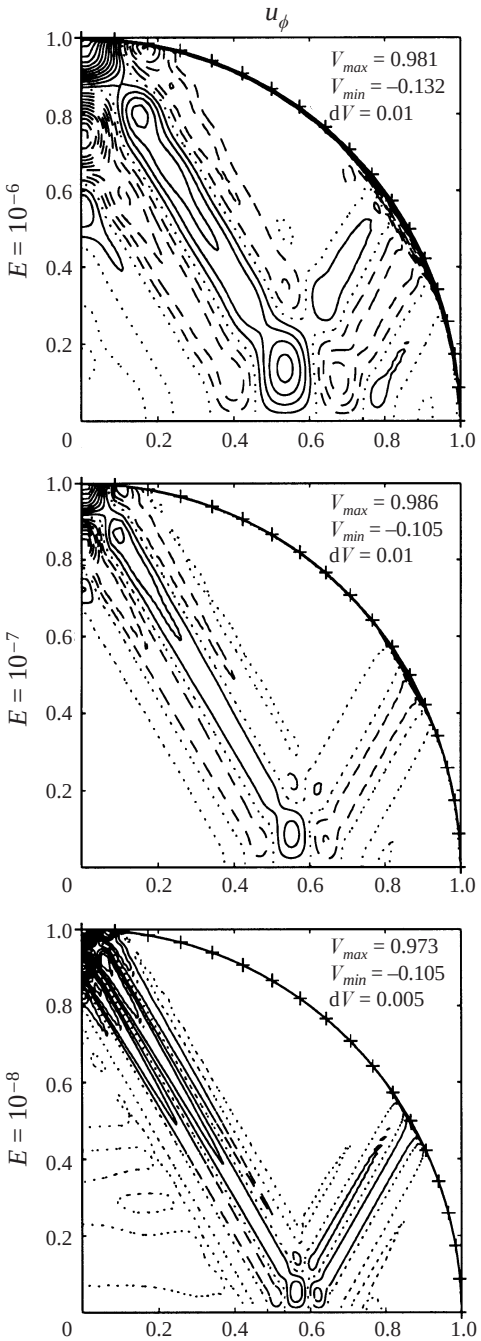

FIGURE 2. The three components of the flow in the meridional plane containing $\hat{\boldsymbol{k}}_c$ and $\boldsymbol{\omega}_1$. Left-hand column: u_r. Middle column: u_θ. Right-hand column: u_ϕ. From top to bottom: $E = 10^{-6}, E = 10^{-7}, E = 10^{-8}$. Contour intervals d$V$, maxima V_{max}, and minima V_{min} are indicated on each figure. —— (– – –), positive (negative) values. · · · · ·, zero isocontour line. Only fifteen isocontour lines are shown and large values are not plotted.

r^*	u^*_ϕ	$\ln(\lvert u^*_\phi\rvert)/\lvert r^*\rvert$	r^*	u^*_ϕ	$\ln(\lvert u^*_\phi\rvert)/\lvert r^*\rvert$
−7.64	0.00034	−1.05	1.07	0.36554	−0.94
−6.69	0.00198	−0.91	2.80	−0.19402	−0.58
−5.75	−0.00179	−1.13	4.11	0.03195	−0.84
−4.92	0.00386	−1.11	5.05	−0.01050	−0.90
−3.93	−0.01639	−1.05	5.89	0.00171	−1.05
−2.68	0.08951	−0.90	6.55	−0.00153	−1.02
−1.10	−0.31819	−1.05	7.14	0.00035	−1.02

TABLE 1. Distance to the characteristic surface and value of the extrema of $u^*_\phi = E^{-1/5}u_\phi$ (as inferred from figure 3). $r^* = E^{-1/5}(r-0.5)+0.5$. $E = 10^{-8}$. The third columns show exponential decay of the velocity amplitude away from the characteristic surface located at $r^* = 0$.

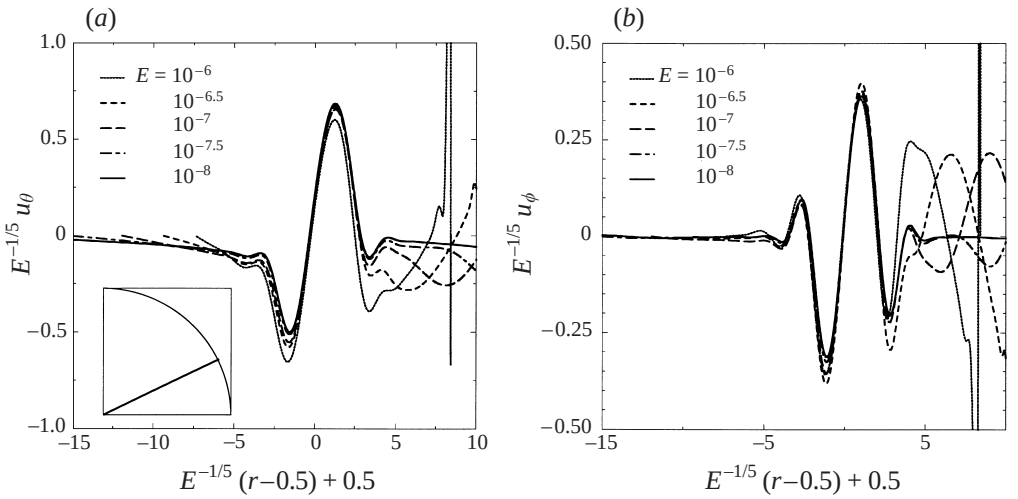

FIGURE 3. Structure of the internal shear layer at $\theta = \frac{1}{3}\pi$, for which the radial direction is normal to the characteristic surface ($r = 0.5$). The radial coordinate is stretched by the factor $E^{-1/5}$. A diagram showing the cross-section in a meridional plane is inserted into (*a*). (*a*) $E^{-1/5}u_\theta$, (*b*) $E^{-1/5}u_\phi$ as a function of the distance to the characteristic surface, for different values of the Ekman number E. Shear in the boundary layer (here of width $O(E^{2/5})$) causes spikes on the left-hand side of both figures for $E = 10^{-6}$.

circle. Retaining both the radial and the tangential derivative $\partial/\partial\theta$, they obtain:

$$(1 \pm 2\cos\theta)\frac{\partial u_\pm}{\partial r} = -\mathrm{i}E\frac{\partial^3 u_\pm}{\partial r^3} \pm \frac{2\sin\theta}{r}\frac{\partial u_\pm}{\partial\theta} \quad \text{with} \quad u_\pm = u_\theta \pm \mathrm{i}u_\phi. \tag{3.3}$$

Away from the critical circles ($2\cos\theta_0 = \pm 1$), they recover a classical Ekman layer and the third term can be neglected. In the critical zone (of the Northern hemisphere to be specific), they write ($\theta = \theta_0 + \psi$) in order to transform equation (3.3) into:

$$2\sin\theta_0\psi\frac{\partial u_-}{\partial r} = -\mathrm{i}E\frac{\partial^3 u_-}{\partial r^3} - \frac{2\sin\theta_0}{r}\frac{\partial u_-}{\partial\psi}. \tag{3.4}$$

Thus, they obtain the scaling as $E^{2/5}$ along the radius and $E^{1/5}$ in the θ-direction. In our problem, the horizontal velocity scales as $\varepsilon = \omega_1 = |\boldsymbol{\omega} - \hat{\boldsymbol{k}}_c|$, where $\boldsymbol{\omega}$ is the solid-body rotation in the interior. From the mass conservation equation, it follows

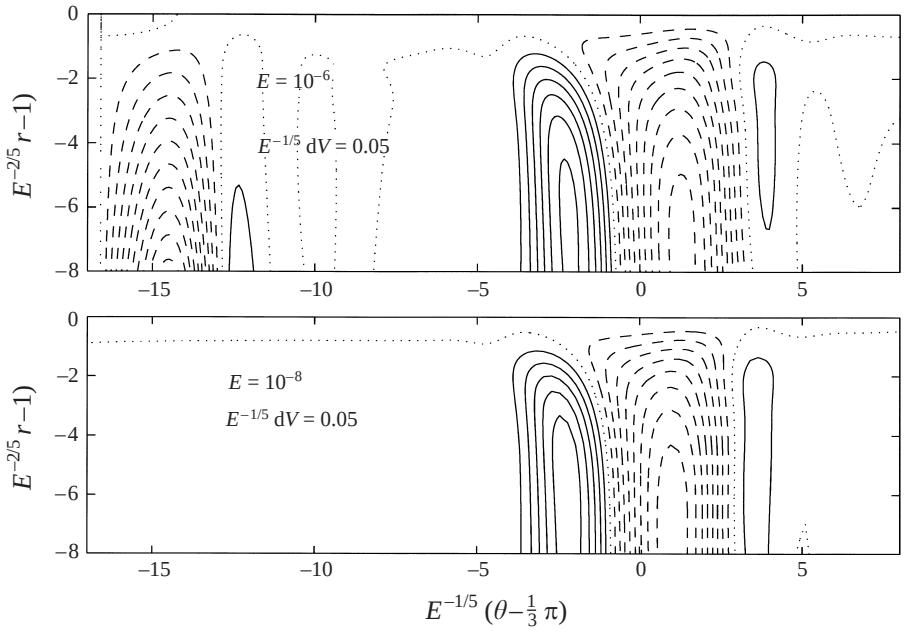

FIGURE 4. Scaling of the boundary layer around the critical latitude ($\theta = \pi/3$). Radial velocity, scaled by $E^{1/5}$, as a function of the latitude and the distance to the surface. Top (bottom) figure: blow-up of the solution for $E = 10^{-6}$ ($E = 10^{-8}$). Same isocontour lines for the two figures.

that u_r is $O(\varepsilon E^{1/5})$ (Stewartson & Roberts 1963). Figure 4 illustrates these different scalings.

That explains the amplitude of the velocity field along the characteristic surfaces. The remaining $O(\varepsilon E^{1/5})$ discontinuity in the horizontal components would be removed at the next order of an expansion in powers of $E^{1/5}$. This result differs from the predictions ($E^{3/10}$ scaling, algebraic decay) based on an analytical study of the coaxial disk system. Kerswell (1995) applied the work of Walton (1975), who had studied the inertial waves propagating from an abrupt discontinuity in the boundary conditions, to the singularity associated with the breakdown of the Ekman layer at 30° latitude. A first difficulty arises because of the spherical geometry of our model. In the coaxial disk system and in an oblate spheroid as well, the characteristic surfaces meet the boundary away from the rotation axis; reflection of the wave generates another shear layer as do subsequent reflections on the boundary. At each reflection, energy is dissipated in the boundary layer. Such a phenomenon does not take place in the sphere and this makes the spherical problem special. On the other hand, we think that the origin of the discrepancy between the prediction by Kerswell (1995) of the velocity along the characteristics and our results can be traced to the modelling by this author of the singularity as a change in the boundary conditions, on an $O(E^{1/5})$ distance, for the tangential velocity field.

4. Nonlinear study of the full precession problem

4.1. *Symmetry of the solution*

As noted in § 2, the boundary conditions are symmetric under parity transformation. On the other hand, Vanyo *et al.* (1995) and Vanyo & Dunn (2000) did observe motions

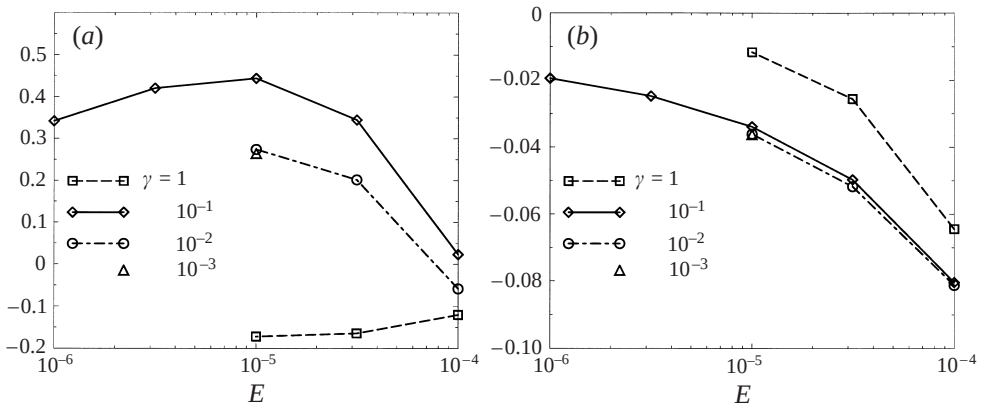

FIGURE 5. Comparison between the numerical determination and the theoretical expression, as given by (4.1), of the equatorial components of the rotation vector $\boldsymbol{\omega}$. Relative differences are shown, with the rotation unit given by (4.1), as a function of the Ekman number E. (*a*) Equatorial component in the meridional plane defined by $\hat{\boldsymbol{k}}_c$ and $\hat{\boldsymbol{k}}_p$, (*b*) $\hat{\boldsymbol{k}}_c$ and $\hat{\boldsymbol{k}}_c \times \hat{\boldsymbol{k}}_p$.

symmetric about the axis of rotation that cross the equatorial plane. These motions do not share the parity symmetry of the boundary conditions. They can arise only as a result of a symmetry-breaking bifurcation. As Tilgner (1999*b*), we have found no evidence of such a bifurcation. It is possible also that we have neglected forces (such as buoyancy) that are important in laboratory experiments.

4.2. *Comparison of the fluid solid-body rotation with Busse's prediction*

In the case of the spherical cavity the expression derived by Busse (1968) for $\boldsymbol{\omega}$ reduces to

$$\boldsymbol{\omega} = \omega^2 \left(\hat{\boldsymbol{k}}_c + \gamma \frac{2.62\omega^{1/2}\, \hat{\boldsymbol{k}}_c \times \hat{\boldsymbol{k}}_p + \hat{\boldsymbol{k}}_c \times (\hat{\boldsymbol{k}}_p \times \hat{\boldsymbol{k}}_c)(0.259\omega^{-1/2} + \gamma \hat{\boldsymbol{k}}_p \cdot \hat{\boldsymbol{k}}_c)}{(0.259\omega^{-1/2} + \gamma \hat{\boldsymbol{k}}_p \cdot \hat{\boldsymbol{k}}_c)^2 + 2.62^2\omega} \right), \qquad (4.1)$$

with $\gamma = \Omega_p E^{-1/2}$. This expression involves only the dimensionless number γ because we have restricted the general expression of Busse (his expression (3.19)) to the case of the spherical cavity. Busse showed that this expression is valid when $\gamma \sin\alpha \ll 1$, where α is the angle which $\hat{\boldsymbol{k}}_p$ makes with $\hat{\boldsymbol{k}}_c$. The calculations are for $\alpha = 23.5°$.

Figure 5 presents a comparison between the numerical determination of $\boldsymbol{\omega}$ and the analytical prediction. Very small values of the Ekman number must be considered to show convergence to the theoretical limit. On the other hand, the component along $\hat{\boldsymbol{k}}_c$ is not displayed as it is very well recovered. The difference between the numerical estimate of $\boldsymbol{\omega} \cdot \hat{\boldsymbol{k}}_c$ and the value predicted by (4.1) scales as γ^2. Busse's equation still gives a fair approximation of the solution for $\gamma = 1$. As γ is further increased, the solid-body rotation ceases to predominate over other motions and indeed it has proved impossible to calculate a numerical solution for equation (2.1) with $\boldsymbol{\omega}$ given by (4.1) for $\gamma = 10$ and $E \leqslant 10^{-4.5}$. The agreement between (4.1) and our numerical determination shows again (see § 3.1) that the singularity of the Ekman boundary layer at the critical circles does not affect the viscous correction to the spin-over mode $(2, 1, 1)$ calculated as an expansion in powers of $E^{1/2}$.

The differential rotation between the interior flow and the solid boundary spawns once again oblique internal shear layers. We rely on the linear calculations, performed

E	δu_ϕ	δs	u_ϕ	s
10^{-5}	0.8×10^{-4}	0.192	0.17×10^{-4}	0.135
$10^{-5.5}$	1.15×10^{-4}	0.147	0.21×10^{-4}	0.116
10^{-6}	1.61×10^{-4}	0.121	0.23×10^{-4}	0.085

TABLE 2. Geostrophic flow. δu_ϕ is the jump of the geostrophic velocity across the cylinders attached to the critical circles, and δs is the radial distance between the velocity extrema on either side of the shear layer. The last two columns give the amplitude and the position of the peak located near the axis.

at much smaller Ekman number, to describe these structures. The novel feature is the geostrophic shear.

4.3. *Geostrophic shear*

As long as equation (4.1) is valid, we can identify the amplitude ε of the boundary-layer flow with $\gamma \sin\alpha$. Figure 6 shows the part of the flow symmetric around $\boldsymbol{\omega}$ for $\gamma = 0.1$. The flow is almost completely geostrophic. It is mainly azimuthal and it is very much invariant in the $\boldsymbol{\omega}$ direction. The numerous strong axial shear layers found by Hollerbach & Kerswell (1995) (their figure 4), in their study of the unforced spin-over mode, are not recovered. The meridional component is confined to the boundary layer in the critical region as the Ekman number is decreased. Figure 7(*a*) shows the geostrophic component as a function of the distance to the $\boldsymbol{\omega}$ axis, again for $\gamma = 0.1$. With decreasing Ekman number, the axial shear becomes localized on the cylinder intersecting the boundary at the critical circles, at a distance $\cos(\frac{1}{3}\pi)$ from the axis. As predicted by Busse (1968), the geostrophic velocity scales as γ^2 (figure 7*b*). This steady interior circulation arises in response to nonlinear effects in the viscous boundary layer. According to Busse, away from the singularity, it becomes independent of the Ekman number in the limit of vanishing E. Our calculations are for Ekman numbers too high to show this behaviour unambiguously. On the other hand, we find that the width of the shear layer scales as $E^{1/5}$ (see table 2). Hence, it is defined by the size of the singularity at the boundary. Viscous effects in the interior do not play a dominant role because they would smooth the shear on $O(E^{1/4})$ distances (Stewartson 1966; Moore & Saffman 1969) small compared to the lateral extension of the singularity. Finally, we find that the velocity jump across the shear layer shows a dramatic increase as the Ekman number is lowered. The amplitude of the geostrophic velocity $\boldsymbol{u}_G$ in the axial layer attached to the critical circles follows from a comparison of the orders of magnitude.

As noted by Busse (1968), the angular velocity of the container parallel to $\boldsymbol{\omega}$ is equal to ω. As a result, the component of $\boldsymbol{u}$ that is symmetric around $\boldsymbol{\omega}$ vanishes at the boundary. A classical Ekman boundary layer of $O(E^{1/2})$ thickness sets in when an axially symmetric interior circulation is present. In the critical regions, this layer is interior to the boundary layer for the oscillating flow. The viscous drag on the ends of the geostrophic cylinders can be determined by considering the flux in the boundary layer. It scales as $E^{1/2}\boldsymbol{u}_G$. On the other hand, the dominant nonlinear terms in the ϕ-direction, in the $O(E^{2/5})$ boundary layer are

$$u_r \frac{\partial u_\phi}{\partial r} + \frac{u_\theta}{r}\frac{\partial u_\phi}{\partial \theta}. \tag{4.2}$$

Since the tangential and radial velocities in the critical region are, respectively, $O(\gamma)$

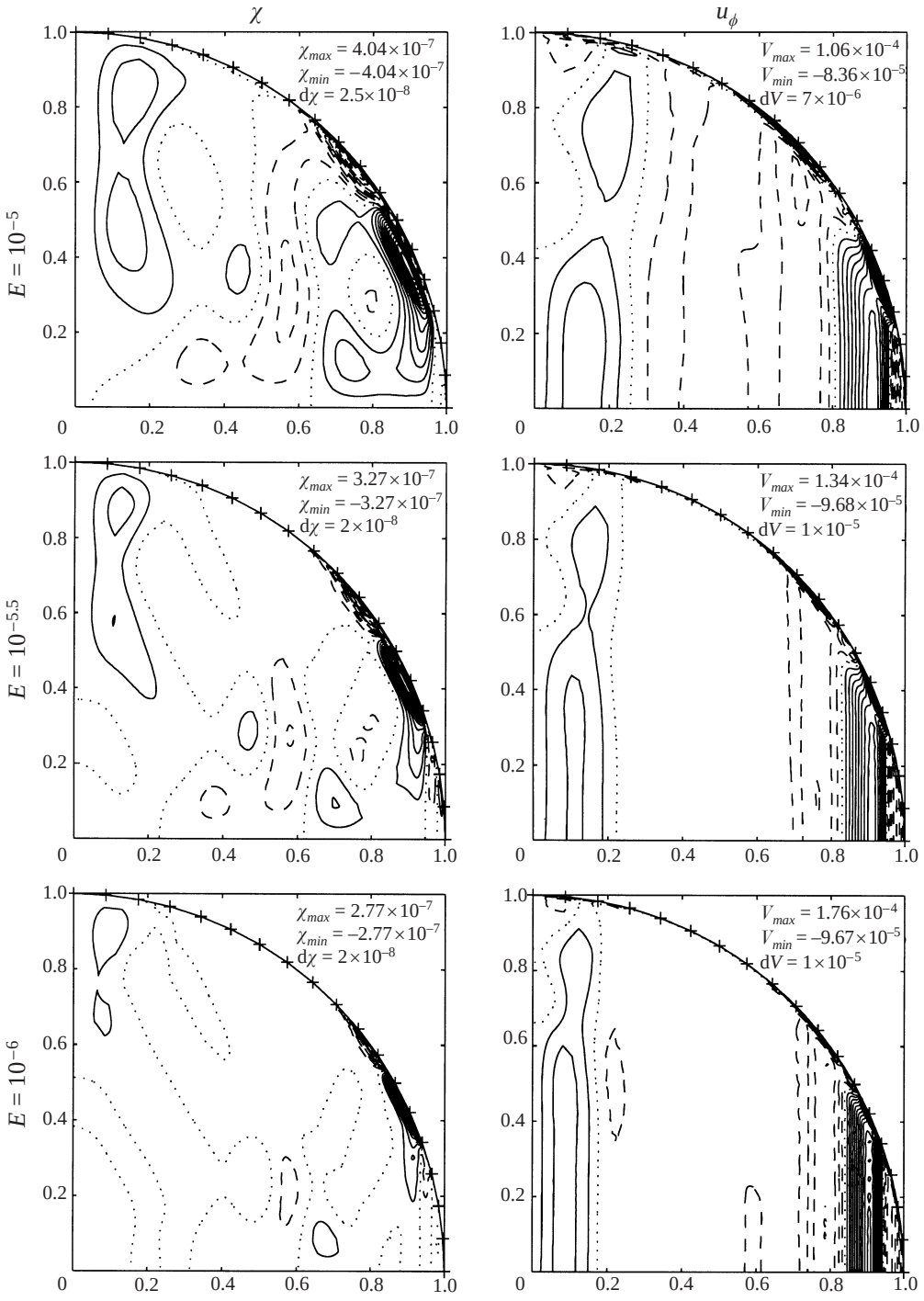

FIGURE 6. Axisymmetric component $\hat{\boldsymbol{e}}_\phi \times \nabla(\chi(r,\theta)) + u_\phi(r,\theta)\hat{\boldsymbol{e}}_\phi$ of the flow in a precessing sphere ($\hat{\boldsymbol{e}}_\phi$ is the unit vector in the azimuthal-direction). Left-hand column: meridional flow χ. Right-hand column: azimuthal velocity u_ϕ. From top to bottom: $E = 10^{-5}$, $E = 10^{-5.5}$, and $E = 10^{-6}$. $\gamma = 0.1$. Contour intervals dV and $d\chi$ are indicated.

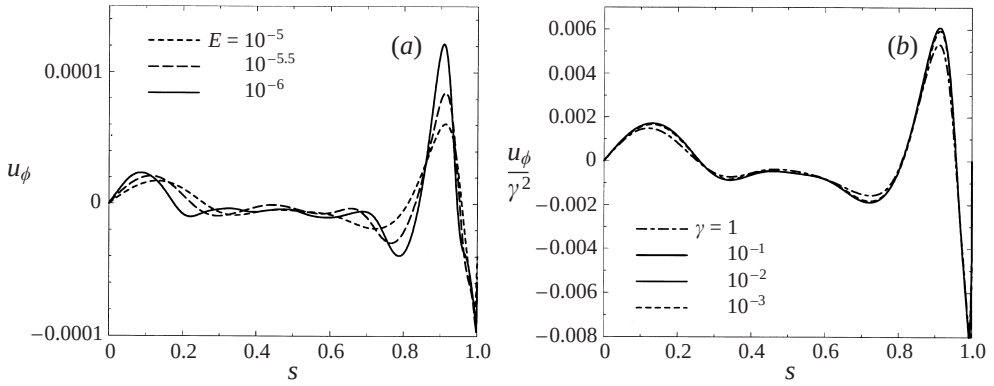

FIGURE 7. Geostrophic velocity as a function of the distance to the axis of the fluid solid-body rotation. (*a*) $\gamma = 0.1$ and E varies from 10^{-5} to 10^{-6}. (*b*) $E = 10^{-5}$ and γ varies from 1 to 10^{-3}. The geostrophic flow is scaled by γ^2.

and $O(\gamma E^{1/5})$, the amplitude of the nonlinear effects amounts to $\gamma^2 E^{-1/5}$ in a layer of $O(E^{2/5})$ thickness. It follows that the geostrophic velocity scales as $\gamma^2 E^{-3/10}$. Finally, table 2 (second column) shows that the $E^{-3/10}$ scaling for the geostrophic circulation is definitely buttressed by the numerical evidence. The numerical exponent inferred from the values reported in table 2 is 0.30. In addition to the shear layer identified by Busse, we find some weak shear, distributed in the interior. It is tiny in comparison with the main shear except in the vicinity of the rotation axis.

5. Discussion

We now compare our numerical results with experimental observations, which have been obtained in oblate spheroids. We have shown that the oscillating layers and also the geostrophic circulation are the consequences of differential rotation between the fluid and its container. Busse (1968) discussed the region in the parameter space for which the fluid motion is predominantly a solid-body rotation. According to Busse (1968), a measure of our parameter γ is given by the smallest of the two quantities $\Omega_p E^{-1/2}$ and $\Omega_p \eta^{-1}$, where η is the flattening. His theory applies as one of these two parameters is small compared to 1 (but see also the recent numerical results of Tilgner & Busse (2001) for $\gamma > 1$ in a spherical shell). With $\Omega_p \eta^{-1} \ll \Omega_p E^{-1/2}$, the expression derived by Busse (1968) for $\boldsymbol{\omega}$ reduces to

$$\boldsymbol{\omega} = \omega^2 \hat{\boldsymbol{k}}_c + \Omega_p \eta^{-1} \hat{\boldsymbol{k}}_c \times (\hat{\boldsymbol{k}}_p \times \hat{\boldsymbol{k}}_c), \tag{5.1}$$

and the parameter γ is estimated as 2.62 $\Omega_p \eta^{-1}$ instead of $\Omega_p E^{-1/2}$. We have thus obtained a way to transfer results obtained in the spherical case to the ellipsoidal case. According to § 3.2, the velocity in the oscillating internal shear layers scales as $\gamma E^{1/5}$ whereas the steady geostrophic velocity scales as $\gamma^2 E^{-3/10}$ (see § 4.3). However, equations (4.1) or (5.1) become less accurate as $\Omega_p E^{-1/2}$ or $\Omega_p \eta^{-1}$ are comparable or of order 1. Hence, in order to compare the experimental measurement of Malkus (1968) of the geostrophic velocity ($\gamma = 0.8$, see below) with our numerical prediction, we do not rely on (5.1). Instead, we use the solvability condition (3.14) of Busse (1968) to infer the equatorial component of the differential rotation from the measured axial component (the average westward drift of the dye line photographed by Malkus). Then, we rely on our numerical calculation and on the $E^{-3/10}$ scaling to predict the

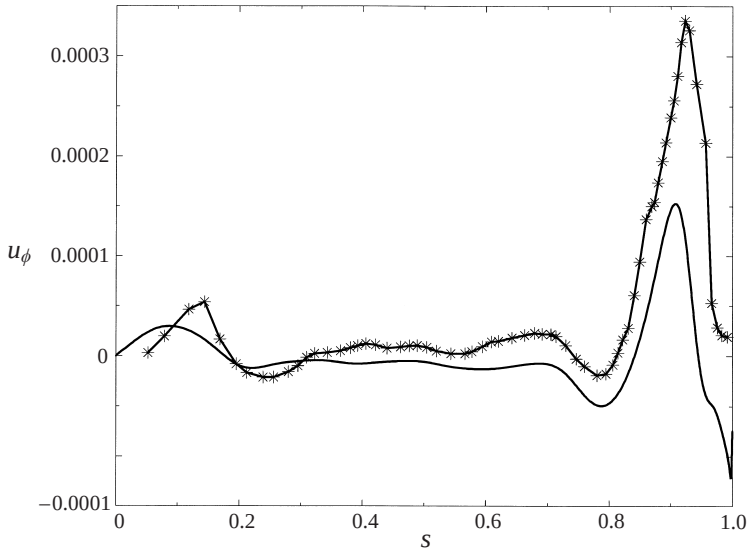

FIGURE 8. Geostrophic velocity as a function of the distance to the axis of the fluid solid-body rotation. Stars correspond to the Malkus experimental data. The solid line is deduced from the numerical results ($\gamma = 0.1, E = 10^{-6}$) and the observed axial differential rotation between the fluid and its container (see text).

geostrophic circulation from the equatorial rotation for $E = 2.5 \times 10^{-6}$, the Ekman number in the Malkus experiment. Figure 8, which is drawn after the figure 3 (left) of Malkus (1968), shows good agreement between our numerical findings in a full sphere and the experimental results in an ellipsoidal cavity. Because the oblique oscillating layers have $O(E^{1/5})$ thickness, we suspect indeed that the flattening η is negligible, except for the determination of the differential rotation, as $\eta \ll E^{1/5}$.

On the other hand, the inertial waves, that are conspicuous in the numerical solutions, have never been visualized in precession experiments (Malkus 1968; Vanyo *et al.* 1995). Vanyo *et al.* (1995) used a shell of flattening $\eta = 1/100$. The precession axis makes an angle $\alpha = 23.5^\circ$ with the rotation axis as in the geophysical case and our calculation. The rotation rate of the spheroid was held constant. It corresponded to an Ekman number $E \sim 8 \times 10^{-7}$. With these figures, we find that $\eta \ll E^{1/5}$. Vanyo *et al.* (1995) varied the precession rate by two orders of magnitude. For the smallest value of Ω_p, we find $\gamma = 0.13$ and the theory of Busse (1968) applies. The set of parameters representative of the Vanyo *et al.* experiment is close to a set ($\gamma = 0.1; E = 10^{-6}$) discussed at length in § 4.3. For this numerical solution, the velocity inside the oblique shear layers is 20 times larger than the steady geostrophic circulation. Neither did Malkus (1968) observe the oblique shear layers. With ($\gamma = 0.8; E = 2.5 \times 10^{-6}; \alpha = 30^\circ$), we still expect the velocity along the characteristic cones to be three times larger than the geostrophic velocity. Hence, it is likely that these layers have not been visualized because of their oscillatory nature and, indeed, McEwan (1970) had to rely on sophisticated methods to see these layers in a rotating fluid cylinder.

Until the work of Vanyo & Dunn (2000), the experiments had not included an inner core, which may be important for the geophysical application. The flow in a precessing spherical shell has been recently investigated numerically by Tilgner (1999*b*). His study has encompassed the effect of an imposed magnetic field on the flow. The solution of Tilgner is dominated by internal layers driven by the shear at the inner core boundary

(see also Hollerbach & Kerswell 1995; Rieutord & Valdetarro 1997; Tilgner 1999*a*). The axisymmetric component of the flow mainly features oblique shear layers that are probably the result of nonlinear interaction of the flow in the internal oscillating layers attached to the inner core at the critical circles. In our view, the emergence of oscillating layers from the boundary with the inner sphere is not yet fully understood but, in any event, the velocities in these layers are small compared to γ (Tilgner (1999*b*) has assumed that the two boundaries are corotating). It follows that the velocities in the oblique axisymmetric layers are small compared to γ^2 and are negligible to the $O(\gamma^2 E^{-3/10})$ geostrophic velocity in the axial shear layer attached to the critical circles of the outer boundary. The latter layer dominates the axisymmetric part of the flow in the asymptotic limit of small Ekman numbers and it is possible that, in a spherical shell, this occurs only at much smaller Ekman numbers than numerically attainable. Thus, we anticipate that our conclusions about the axial layer are valid also for a model including an inner core, and it seems indeed than an axial layer shows up, not far from the critical circles, in the solution of Tilgner (1999*b*) (his figure 8*a*, right), as the Ekman number is decreased. Finally, we may ponder on the existence of another axial cylindrical layer attached to the critical circles of the inner boundary.

In the Earth's core, the value of the dimensionless numbers that are important to determine the effects of the mantle precessional motion are ($\eta = 1/400$, $\gamma = 1.1 \times 10^{-4}$, $E = 10^{-15}$). Thus, the $O(E^{1/5})$ width of the shear layers is not very small compared to the flattening η. The numerical modelling yields a prefactor of order one for the thickness of these layers. As a result, the inertial waves spawned by the breakdown of the outer boundary layer in the Earth's core are perhaps best modelled in the oblate spheroid geometry. On the other hand, the most significant feature, from the geophysical viewpoint, is the steady axial shear. The mechanism behind the development of this interior circulation does not depend on the ellipticity, of which the only role is to determine the value of the parameter γ. From the numerical values above and the scaling laws determined in § 4.3, it follows that $\boldsymbol{u}_G = 3 \times 10^{-5}\,\mathrm{m\,s^{-1}}$. It is comparable to the velocities of the core surface motions inferred from the secular variation of the Earth's magnetic field ($10^{-4}\,\mathrm{m\,s^{-1}}$). On the other hand, the magnetic Reynolds number based on u_G and the thickness of the axial layer is only 10^{-1}, implying that magnetic field generation in the shear layer itself is unimportant.

We thank A. Pais and J.-L. Le Mouël for many stimulating and valuable discussions. All the computations presented in this paper were performed at the Service Commun de Calcul Intensif de l'Observatoire de Grenoble. We acknowledge support from the programme Intérieur de la Terre of CNRS/INSU.

Appendix. Numerical method

Since the fluid we consider is incompressible, the velocity field $\boldsymbol{u}$ can be expressed in terms of poloidal and toroidal functions:

$$\boldsymbol{u} = \nabla \times (T\boldsymbol{r}) + \nabla \times \nabla \times (P\boldsymbol{r}), \tag{A 1}$$

where $\boldsymbol{r}$ is the position vector. We expand P and T as

$$P = \sum_{l \leqslant L, m \leqslant min(l,M)} F_l^m(r,t) Y_l^m(\theta,\phi), \tag{A 2}$$

$$T = \sum_{l \leqslant L, m \leqslant min(l,M)} G_l^m(r,t) Y_l^m(\theta,\phi), \tag{A 3}$$

where (r, θ, ϕ) are spherical coordinates, t is time, L and M are truncation levels,

$$Y_l^m(\theta, \phi) = C_l^m P_l^m(\cos(\theta)) e^{im\phi}, \tag{A 4}$$

$P_l^m(\cos(\theta))$ denotes associated Legendre functions, and C_l^m is a coefficient of normalization. Let us define $\hat{\boldsymbol{e}}_z = \boldsymbol{\omega}/\omega$. Operating with $\boldsymbol{r} \cdot \nabla\times$ and $\boldsymbol{r} \cdot \nabla \times \nabla\times$ on (2.1), we obtain the following set of equations for T and P:

$$\begin{aligned}\left(E\nabla^2 - \frac{\partial}{\partial t}\right) L_2 T + 2\omega\,(\hat{\boldsymbol{e}}_z \times \boldsymbol{r}) \cdot \nabla T - 2\omega Q_3 P - 2\boldsymbol{r} \cdot (\Omega_p \hat{\boldsymbol{k}}_p(t) \times \omega) \\ = \boldsymbol{r} \cdot \nabla \times (2\Omega_p \hat{\boldsymbol{k}}_p(t) \times \boldsymbol{u} + (\boldsymbol{u} \cdot \nabla)\,\boldsymbol{u}), \\ \left(E\nabla^2 - \frac{\partial}{\partial t}\right) L_2 \nabla^2 P + 2\omega\,(\hat{\boldsymbol{e}}_z \times \boldsymbol{r}) \cdot \nabla\left(\nabla^2 P\right) + 2\omega Q_3 T = -\boldsymbol{r} \cdot \nabla \times (\nabla \times (\boldsymbol{u} \cdot \nabla)\,\boldsymbol{u}).\end{aligned} \tag{A 5}$$

Q_3 and L_2 are classically defined as:

$$Q_3 = \hat{\boldsymbol{e}}_z \cdot \nabla - \tfrac{1}{2}(L_2 \hat{\boldsymbol{e}}_z \cdot \nabla + \hat{\boldsymbol{e}}_z \cdot \nabla L_2), \tag{A 6}$$

$$L_2 = \frac{\partial}{\partial r} r^2 \frac{\partial}{\partial r} - r^2 \nabla^2. \tag{A 7}$$

The boundary conditions are $(r = 1)$:

$$P = T = \frac{\partial P}{\partial r} = 0. \tag{A 8}$$

As in Dormy, Cardin & Jault (1998), we use a Crank–Nicholson scheme for the diffusion term and an Adams–Bashford scheme for all the others. Calculation in the radial direction is by finite-differences. In order to have an accurate enough resolution of the Ekman boundary layer, we increase the number of points in the vicinity of the outer surface, and conversely, we stretch the radial grid at the centre of the fluid to deal with reasonable timesteps and angular resolution. As an example, in order to calculate the flow in a precessing sphere for $\gamma = 0.1$ (see equation (4.1) for the definition of γ) and $E = 10^{-6}$, we use a deformed grid of 1000 radial points (our radial scheme is second-order accurate), with $L = 127$, $M = 7$ and 10^{-2} as the timestep. Calculations in the ϕ direction are fully spectral. Nonlinear terms and the last term on the left-hand side of the first equation (A 5) are calculated by collocation in the θ-direction. The benefits of linearizing (A 5) without neglecting also the terms involving Ω_p would thus be limited.

REFERENCES

Busse, F. H. 1968 Steady fluid flow in a precessing spheroidal shell. *J. Fluid Mech.* **33**, 739–751.

Dormy, E., Cardin, P. & Jault, D. 1998 MHD flow in a slightly differentially rotating spherical shell, with conducting inner core, in a dipolar magnetic field. *Earth Planet. Sci. Lett.* **160**, 15–30.

Greenspan, H. P. 1968 *The Theory of Rotating Fluids.* Cambridge University Press.

Greenspan, H. P. 1969 On the non-linear interaction of inertial modes. *J. Fluid Mech.* **36**, 257–264.

Hollerbach, R. & Kerswell, R. R. 1995 Oscillatory internal shear layers in rotating and precessing flows. *J. Fluid Mech.* **298**, 327–339.

Kerswell, R. R. 1995 On the internal shear layers spawned by the critical regions in oscillatory Ekman boundary layers. *J. Fluid Mech.* **298**, 311–325.

McEwan, A. D. 1970 Inertial oscillations in a rotating fluid cylinder. *J. Fluid Mech.* **40**, 603–640.

Malkus, W. V. R. 1968 Precession of the Earth as the cause of geomagnetism. *Science* **160**, 259–264.

Moore, D. W. & Saffman, P. G. 1969 The structure of free vertical shear layers in a rotating fluid and the motion produced by a slowly rising body. *Phil. Trans. R. Soc. Lond.* A **264**, 597–634.

Poincaré, R. 1910 Sur la précession des corps déformables. *Bull. Astr.* **27**, 321–356.

Rieutord, M. & Valdetarro, L. 1997 Inertial waves in a rotating spherical shell. *J. Fluid Mech.*, **341**, 77–99.

Roberts, P. H. & Stewartson, K. 1963 On the stability of a Maclaurin spheroid of small viscosity. *Astrophys. J.* **137**, 777–790.

Stewartson, K. 1966 On almost rigid rotations. Part 2. *J. Fluid Mech.* **26**, 131–144.

Stewartson, K. & Roberts, P. H. 1963 On the motion of a liquid in a spheroidal cavity of a precessing rigid body. *J. Fluid Mech.* **17**, 1–20.

Tilgner, A. 1999*a* Non-axisymmetric shear layers in precessing fluid ellipsoidal shells. *Geophys. J. Intl* **136**, 629–636.

Tilgner, A. 1999*b* Magnetohydrodynamic flow in precessing spherical shells. *J. Fluid Mech.* **379**, 303–318.

Tilgner, A. & Busse, F. 2001 Fluid flows in precessing spherical shells. *J. Fluid Mech.* **426**, 387–396.

Vanyo, J. P. & Dunn, J. R. 2000 Core precession: flow structures and energy. *Geophys. J. Intl* **142**, 409–425.

Vanyo, J. P., Wilde, P., Cardin, P. & Olson, P. 1995 Experiments on precessing flows in the Earth's liquid core. *Geophys. J. Intl* **121**, 136–142.

Walton, I. C. 1975 Viscous shear layers in an oscillating rotating fluid. *Proc. R. Soc. Lond.* A **344**, 101–110.